# Carrier Transport and Energy Harvesting in ZnO Nanowires

João Pedro Martins Godinho
joao.m.godinho@ist.utl.pt

Instituto Superior Técnico, Lisboa, Portugal

September 2015

**Abstract**

ZnO nanowires have been used to enhance carrier collection in dye sensitized solar cells due to longer optical path with simultaneous ease of carrier collection. Zinc oxide is also interesting for its piezoelectric property, and thus its capability for energy harvesting. We have deposited 100 nm wide and 5 $\mu$m long ZnO nanowires by a wet chemical process, and we compared different transport characteristics of such nanowires with a homogeneous ZnO thin film, focusing on the surface trapping effects. Strong variations of the power law exponent as a function of applied electric field in log-log representations of current-voltage characteristics, is interpreted as a manifestation of transport in the Trap-Filled Limit regime, which lead to estimate the density of deep trap states as $p_{t,0} = 4.4 \times 10^{12}$ cm$^{-3}$ and the concentration of carriers to be $n_0 = 1.5 \times 10^9$ cm$^{-3}$. Transient photocurrent measurements showed a temperature dependence of the photo-response of the nanowires. When deconvoluted using Laplace Transform, the signal yielded two peaks in the density-of-states distribution ascribed to surface trapping at 0.85 eV and 0.95 eV. Admittance spectroscopy showed a peak related to an intrinsic defect at $0.48 \pm 0.02$ eV and at $0.44 \pm 0.02$ eV for the nanowire and thin film sample, respectively.
**Keywords:** Zinc Oxide, Nanowires, Deep-level Defects, Trap-Filled-Limit, Surface Trapping.

## 1. Introduction

Zinc oxide has been attracting intensive research due to its physical and chemical properties, that allow its usage in a wide range of applications.

Research on ZnO for electronic devices started in 1930, and reached its peak in 1980. However, the interest began to fade away owing to the difficulty of doping ZnO in a p-type semiconductor, which is essential to optoelectronic purposes. The reawakening in the researching activity on this compound has begun in the nineties, following the growth of a variety of nanostructures, for instance nanowires, quantum wells and quantum dots, with the aim to obtain the following applications: transparent electronics, ultraviolet (UV) light emitters, piezoelectric devices, chemical sensors, spin electronics [1] and an enduring material under a radiation environment. Doping to p-type has already made some progress, although it is still a major challenge to overcome, in order to have stable and reproducible p-type ZnO [2].

One of the most important properties of ZnO is certainly its piezoelectricity, that arises from the non-central symmetric structure. Due to it, it has been used in force sensing, acoustics wave resonator, acousto-optic modulator applications, among others. The search for sustainable nano-power sources for mobile devices is a promising field of researching, offering solutions to nanodevices. A possible way to obtain such a nano-power source is through the piezoelectric effect. With the aim of converting the kinetic energy of environmental vibrations into electricity, in 2006 the first piezoelectric generator was demonstrated using ZnO nanowires in [3]. Since then, the usage of nanowires in these applications has been thoroughly studied due to their advantages of having high piezoelectric coefficients, high elasticity and high resistance to fatigue [4].

Their electrical properties have also been studied and the results indicate that nanowire-based devices can be operated faster than their thin film counterpart. Furthermore, concerning optical properties, it has been reported that arrays of nanowires have been used as light emitting diodes[4], and it has been shown that quantum size confinement increases the exciton binding energy, which as stated before, increase the efficiency of the emission. In addition, its near-cylindrical geometry and high refractive index make ZnO nanowires a candidate for optical waveguides. Finally, upon adsorption of molecules on the surfaces, the conductivity of the material changes. In n-type materials it often leads to a decrease in conductivity. This is the main principle behind gas sensors. Due to its larger surface to volume ratio, nanowires enhance the gas sensing performance [1].

ZnO has also attracted intensive research due to, for example, its application as window layers in solar cells, either as transparent conductive layers, or as active UV-sensitive front diode in heterostructure solar cells. In particular, in Dye Sensitized Solar Cells (DSSC), nanowires add the advantage of allowing the dye to be attached directly onto the surface, and thus offering to electrons a direct path to the anode, reducing recombination losses and therefore increasing the collection efficiency of the cell.

As a material with interesting properties and a promising role in future technologies, this work focuses on characterization of ZnO nanowires prepared by wet chemical process, by means of studying their carrier transport properties, as well as their capability for energy harvesting. However, most of the work is focused on comparing surface related effects in homogeneous thin films of ZnO with those observed in nanowire structures. Pulsed laser deposition (PLD) and a wet chemical process are used for deposition, respectively. Both types of samples have been characterized by scanning electron microscopy (SEM), photocurrent spectroscopy (PCS), transient photocurrent analysis (TPC), electrical measurements including IV curves and admittance spectroscopy. The results are tested against a model that considers the adsorption of oxygen molecules as the main cause for the samples behaviour. We point out the similarities and differences encountered when applying the model to occupation of deep defects located at the ZnO nanowire surfaces.

## 2. Background

### 2.1. Trap-Filled-Limit Regime

In semiconductor IV characteristics, neglecting the possibility of contact barriers, that is assuming an ohmic contact, there are in general three to four regimes. In a phenomenological way, considering a single set of traps, the following behaviour of the current-voltage curve is expected. For low voltages, the injected carrier concentration is negligible compared to the thermally generated ones, so we have an Ohm's law behaviour. As the voltage increases the injected carriers are captured by the trap level, and once the traps are all filled, the current rises, converging afterwards to the Space Charge Limited Current (SCLC) law or trap free square law. And it can be shown that this rise in current after a discrete set of traps is filled is nearly vertical, which is one of the most remarkable results of this theory, since experimentally such high slope in the current-voltage curve could be misinterpreted as an electrical breakdown in the material. An important quantity is the threshold voltage where the current rises abruptly, which is called the Trap Filled Limit voltage ($V_{TFL}$).

For a single set of traps there are two different situations, the set of traps lies below or above the Fermi level, while no voltage is applied. The first one is simpler, since as carriers are injected the Fermi level moves up, never crossing the set of traps, which is not true in latter case. As a result there is a fourth regime located between the Ohm's law and the TFL regime, denoted Shallow-Trap (ST) regime, which shows a quadratic dependence of the voltage, like the SCLC. Once, the Fermi level crosses the level and the shallow trap is fully occupied, a Trap-Filled Limit regime will be present, followed by the SCLC. In short, the general curves of these two cases may be represented as in the figure 1, where a deep-trap shows the sequence of Ohm - TFL - SCLC, whereas a shallow-trap shows Ohm - ST - TFL - SCLC.

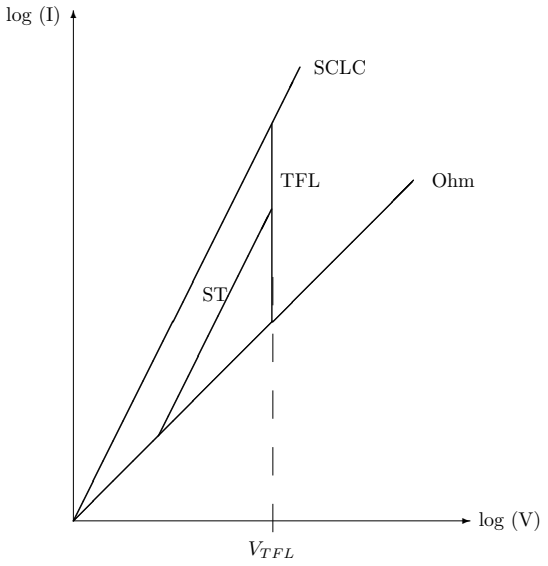


Figure 1: Schematic of a Current-Voltage curve with the four regimes, Ohmic, Space Charged Limited Current (SCLC), Trap-Filled Limit (TFL), and Shallow-Trap (ST) regimes.

Lampert and Mark [5] have developed the model of a single level trap in a semiconductor. According to their model, the regime begins at the designated Trap-Filled Limit voltage $V_{TFL}$, which is given as:

$$V_{TFL} = \frac{e p_{t,0} L^2}{2\epsilon} \quad , \tag{1}$$

where $p_{t,0}$ is the concentration of traps not occupied, e the electron charge, L the space between contacts and $\epsilon$ the electric permittivity of the material. Other important relations from this model are the following ratios:

$$\frac{J_2}{J_1} = 2\frac{p_{t,0}}{n_0} \quad , \tag{2}$$

$$\frac{V_2}{V_1} = \frac{8}{3} \quad , \tag{3}$$

where the subscript 2 denotes the end and 1 the beginning of the TFL regime. Hence, once identified the Trap-Filled Limit voltage $V_{TFL}$ it is possible to obtain an estimation of $p_{t,0}$ and $n_0$.

To clarify the influence of $p_{t,0}$ on the TFL regime and the general curve of this regime, we solved the analytic equation that describes an insulator with a deep trap with various values of $n_0$ and $p_{t,0}$, and plotted the results in figure 2. It was varied the values of $n_0$ and the ratio between the two concentration $A = \frac{p_{t,0}}{n_0}$. Changing the ratio, while keeping $p_{t,0}$ constant, it influences the ohmic regime, as expected since there are more carriers in the material. Besides that it also influences the slope of the TFL regime, which is steeper for higher values of $A$. On the other hand, if the ratio $A$ is kept constant and the value of $p_{t,0}$ is changed (fourth curve), it shifts the curve to higher voltages, thus the voltage at which the TFL begins depends on $p_{t,0}$.

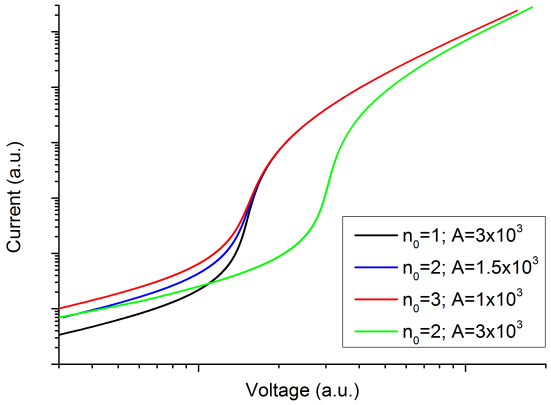


Figure 2: Analytical solution of the single deep trap insulator, using dimensionless variables, for different values of $n_0$ and $p_{t,0} = n_0 A$. Note: These are dimensionless variables.

### 2.2. Piezoelectric Properties

The piezoelectric effect is closely related with the occurrence of electric dipole moments in solids. These dipoles can be induced either due to ions in a crystal lattice that exhibits asymmetries in the charge distribution or by certain molecular groups with electrical properties. Neighbour dipoles tend to have the same direction forming regions called Weiss domains. With a mechanical stress applied, the crystal lattice is displaced and the macroscopic polarization changes. Thus, in these materials there is a coupling between the electric behaviour and the mechanical stress. The opposite effect, applying an electrical field and obtaining a mechanical deformation is known as converse piezoelectric effect.

If no coupling is considered the electric displacement $\vec{D}$ is:

$$[D] = [\epsilon][E] \tag{4}$$

and the strain tensor $S_{ij}$ is given by Hooke's law

$$S_{ij} = s_{ijkl} T_{kl} \tag{5}$$

where $\epsilon$ is the dielectric permittivity tensor, $[E]$ is the electric field vector, $s_{ijkl}$ the compliance (or elastic modulus) tensor and $T_{kl}$ the stress tensor. The elastic modulus is a fourth rank tensor with 81 components, although due to symmetry with respect to suffixes i,j and k,l it reduces the free components to 36. Using Voigt's notation to contract the index pairs i,j and k,l , the Hooke's law may be written in a two rank matrix. To take into account the coupling between the two effects, the electric displacement $\vec{D}$ and the strain tensor $S$ are rewritten as:

$$[D] = [d][T] + [\epsilon^T][E] \tag{6}$$

$$[S] = [s^E][T] + [d]^t[E] \quad . \tag{7}$$

The $[d]$ is the piezoelectric strain constant matrix, the superscripts T and E indicate that these quantities are held constant and the t superscript indicates a transpose matrix. The first equation is known as the direct piezoelectric effect and the second as converse piezoelectric effect. Alternatively, the direct piezoelectric equation may be written as function of the strain:

$$[D] = [e][S] + [\epsilon^T][E] \quad , \tag{8}$$

where $[e]$ is the piezoelectric stress constant matrix. Matrices $[d]$ and $[e]$ are connected by the compliance matrix as $[d] = [s][e]$ [6].

A nanowire is a natural cantilever, and so it can be modelled as a clamped-free beam with circular cross-section, which is statically compressed or bent by a force applied at its free end. Hence, the energy harvesting ability of nanowires can be studied using this simple model.

The main goal is then to calculate the electric potential $\varphi$ that appears in the nanowire, when it is compressed or bent. In order to do so, it was used the following set of equations: the mechanical equilibrium equation:

$$\vec{\nabla}.T = 0 \quad , \tag{9}$$

the piezoelectric effect equations (eq. 6 and 7), and the Gauss equation:

$$\vec{\nabla}.\vec{D} = \rho \quad , \tag{10}$$

where $\rho$ the charge density.

## 3. Materials and Methods

Throughout this work four samples of ZnO nanowires were studied and one additional sample of ZnO thin film in order to compare between

Table 1: Samples studied in this work.

| Sample | Structure | Contact Distance | Growth Method |
|---|---|---|---|
| PS1, PS2 and PS3 | Nanowire | 10 $\mu$m | Chemical bath |
| NWQ | Nanowire | 300 $\mu$m | Chemical bath |
| MEFT4 | Thin film | 300 $\mu$m | PLD |

these two nanostructures. As listed in table 1 samples PS1, PS2 and PS3 are very similar, consisting in nanowires deposited on Corning glass substrates using a wet chemical process. A schematic of these samples is shown on figure 3, illustrating the nanowire layer on top of the gold inter-digital contacts. Notice that the voltage was applied on the contacts *C1* and *C2*. The NWQ sample has a longer contact distance of 300 $\mu$m and instead of being deposited on Corning glass it was prepared on a quartz glass substrate. The reference ZnO film, MEFT4, was deposited on quartz glass substrate by pulsed laser deposition (PLD). All samples have gold metal contcts.

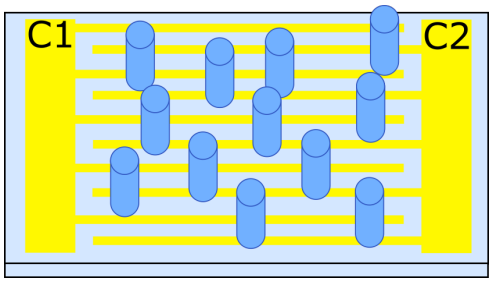


Figure 3: Schematic of the nanowire samples. At yellow we have the gold contacts (C1 and C2) and the cylinders represent the nanowires.

To investigate the optical properties of the structures, particularly the band gap $E_g$ and the Urbach energy $E_u$, photocurrent spectroscopy was performed. To make sure the sample reached a quasi steady state, after selecting a new wavelength and the acquiring the current there was an interval of 12 minutes. The voltage was supplied by a lock-in amplifier, which connected to the acquisition computer by GPIB, and the current reading was done using a Keithley 6485 picoammeter also connected to the computer by GPIB. It was used an optical system to focus the light on the sample, which consisted in optical lenses and a monochromator that was controlled by the acquisition routine written in Labview. The light source used was a 75 W Xe lamp.

Considering the model developed by Lampert and Mark, the IV characteristics were measured in order to investigate the defects states in the samples. Studying the slopes present in the IV curves and determining at which voltage the TFL regime starts, it is possible to infer about the depth of the trap (shallow or deep trap) and estimate the concentration of unoccupied trap states $p_{t,0}$ and the carrier concentration $n_0$.

To further investigate the defects in the nanowire structure, transient photocurrent (TPC) and admittance spectroscopy (AS) were performed at different temperatures. Both techniques give us insight about the defects and traps levels within the material. Furthermore, by performing TPC for a long interval of time and AS for high frequencies, these two techniques become complementary. Since the TPC will be sensible to traps with long emission times and AS to the shorter ones. Thus, at the end one obtains a wide range in emission times, where each peak or distribution can be associated to a given trap level.

It was used the same setup as in PCS, but the monochromator was removed, increasing this way the intensity of light on the sample. Once the light source was turned off, the current flowing through the sample was monitored for a full hour, while the voltage across the sample was kept constant at 0.1 V. A Peltier cell and a thermocouple were used to set and read the sample temperature.

In order to measure the capacitance of the samples it was used a Solartron 1260 impedance analyser, with which the real and imaginary parts of the impedance were measured. Then considering the sample as a resistance in parallel with a capacitor, the resistance and capacitance were deduced. The measurements were obtained using a zero bias voltage, a 0.1 V modulation voltage and 15 s of acquisition time. In order to study the effect of surface trapping, the sample was placed inside the vacuum chamber, and the measurements were firstly made at atmospheric pressure and afterwards in vacuum conditions at $10^{-3}$ mbar.

## 4. Results and Discussion

In this chapter we present the main results and will propose a model to explain those findings.

This work started with the five samples aforementioned. However, not all measurements were made with each sample. Due to the fact that, PS1 and PS2 got damaged during a transient photocurrent experiment, where it was used a Nd:YAG laser system. In an attempt to have a nanowire sample with the same contact distance as the reference sample, the ZnO thin film (MEFT4), the sample NWQ was made. However, it showed a higher resistance when compared with the other nanowire samples. While at room temperature PS1, PS2 and PS3 show values around 300 $\Omega$, NWQ showed 5 M$\Omega$. Furthermore, with usage its value increased. This might mean that the deposited metal contact was not thick enough, so that maybe it was not uniform and likely over the various measurements the contacts got damaged. Therefore, special focus will given to the results from PS3 and MEFT4, and in

this extended abstract of the thesis only results of these two samples will be shown.

### 4.1. Morphology

The nanostructures grown with this method have approximate lengths of 5 $\mu$m and widths of 100 nm. SEM images show a wide variety of flakes, nanowires and crystallites. In some images there are some bunches of nanowires on top of a first layer of nanowires. These bunches may have grown in the solution and then got deposited on top of the other, or due to some impurities or defects they started to grow on top of them. Figure 4 shows two SEM images of PS3 with different magnifications.

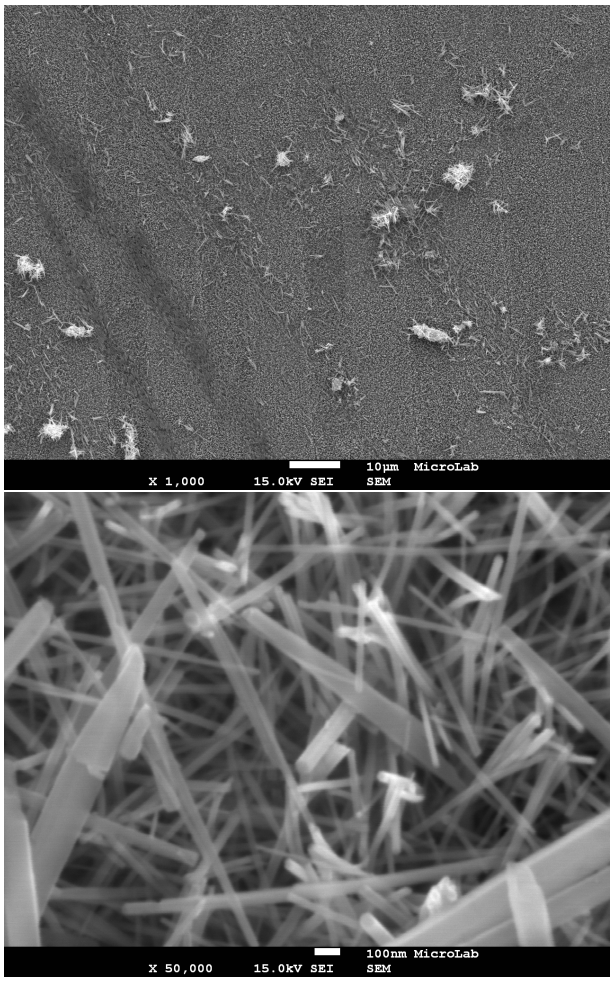


Figure 4: SEM images of PS3.

### 4.2. Energy Harvesting

From the set of equations described before (eq. 6 to 10) it was studied two possible configurations to harvest energy from nanowires, axial compression and bending. For the first case an analytical expression was obtained:

$$V = -\frac{e_{33}}{\epsilon_{33}}\frac{F}{EA}l \quad , \tag{11}$$

where $V$ is the electric potential generated, $e$ the piezoelectric coefficient matrix, $\epsilon$ the electric permittivity, $F$ the applied force, $E$ the Young modulus and $A$ the cross section of the nanowire. The other configuration lead to a Poisson equation $\nabla^2\varphi = -\frac{\rho}{\epsilon_{11}}$ that was solved numerically, where the charge density is given by:

$$\rho = \frac{F}{EI}y\left[e_{33} - 2\nu e_{31} - e_{15}(1+\nu)\right] \quad , \tag{12}$$

with $I = \frac{\pi}{4}r^4$, $r$ the radius of the nanowire and $\nu$ the Poisson coefficient.

Considering nanowires with 5 $\mu$m length and 100 nm width and an applied force of 80 nN, the compression configuration yielded 5.5 V while the bending the nanowire results in 0.05 V. Figure 5 shows the solution to the Poisson equation obtained with these parameters. The value of each constant used was: $E = 142$ GPa, $\nu = 0.323$, $\epsilon_{11} = \epsilon_{22} = 7.77$, $\epsilon_{33} = 8.91$, $e_{31} = -0.543$ Cm$^{-2}$, $e_{33} = 1.203$ Cm$^{-2}$ and $e_{15} = -0.444$ Cm$^{-2}$.

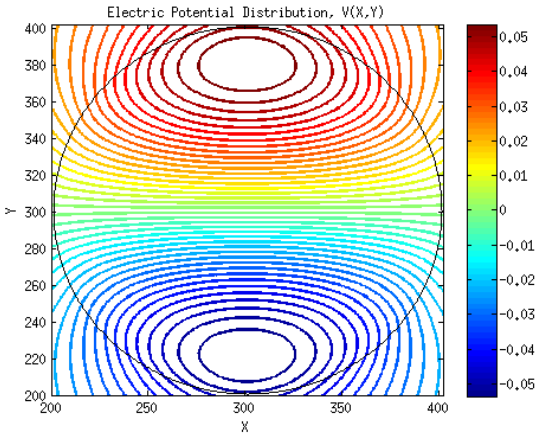


Figure 5: Electric potential within a nanowire when it is bent. The axis X and Y are indices of the grid used to solve the Poisson equation, and the circle defines the nanowire.

It is possible to conclude that regarding the energy harvesting, the nano-generators based in axial compression are more efficient, as well as those that whose nanowires are thinner and taller. Furthermore, the axial compression shows a linear response, which makes this nanostructure useful for force sensing, owing to this sought property in any sensor.

### 4.3. Photocurrent Spectroscopy

The photocurrent spectrum obtained for PS3 is in figure 6. Thus, assuming that the photocurrent, that is, the difference between total and dark current, is proportional to the absorption coefficient, a Tauc plot of the form $(I_{ph}h\nu)^2$ was performed. It yielded a band gap energy of 3.2±0.3 eV, which is in

agreement with the literature. From this spectrum the Urbach Tail was also estimated to be around the $33 \pm 1$ meV, which indicate a good crystalline structure.

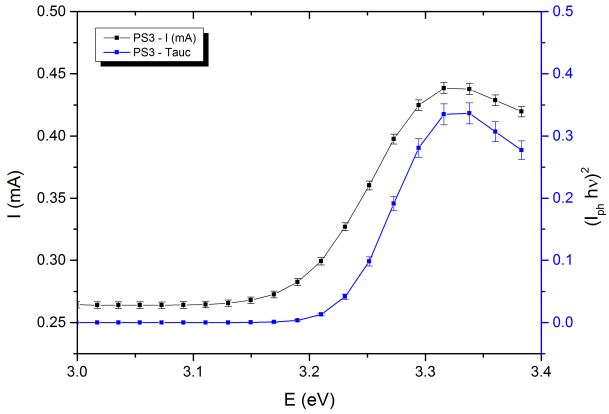


Figure 6: Photocurrent spectrum and Tauc plot of PS3.

### 4.4. Current-Voltage Characteristics

The results for the PS3 are presented in the figure 7, where various Current-Voltage (or IV) curves were obtained at different temperatures. The first thing to note is the clear change in behaviour after 0.5 V, especially for lower temperatures. Firstly, in the first regime, for all temperatures analysed (temperatures lower than 28°C were excluded as their signals for low voltages are within the noise), the slope in the log-log representation is compatible with or near 1. Thus, this is the ohmic regime, meaning that there is a negligible injection barrier.

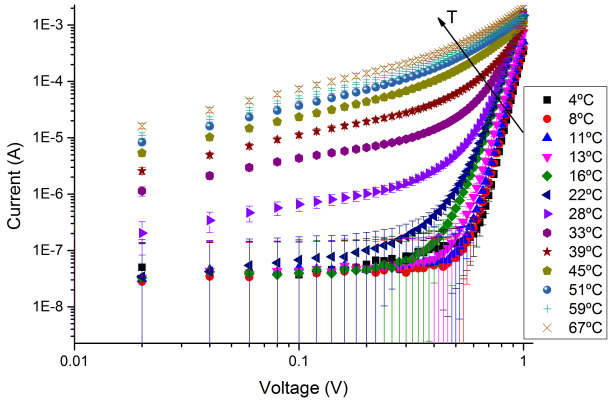


Figure 7: Current-Voltage curves of PS3 at various temperatures.

At high temperatures, the slope approaches the value of 2, which is the expected value for a SCLC regime. This supports the hypothesis of low trap concentration at high temperatures, as an ideally trap-less semiconductor would go from ohmic to SCLC, without presenting a TFL behaviour. Either that or a given deep trap is only present at low temperatures, and at high temperatures it vanishes, leaving behind a dominant shallow trap level. In order to know which hypothesis is correct, a possible solution would be to scan over a wider range in voltages, and look whether the slope keeps approximating the value 2 or if it is observed a TFL behaviour. The first would mean the sample is in a SCLC regime and the second one would mean a Shallow Trap regime.

The estimation of the concentration $p_{t,0}$ comes from the crossover voltage, that is, the voltage at which the sample changes from ohmic to TFL. Regarding this estimation, the results were not so conclusive due to the limitation in measuring at low temperatures, where the TFL regime is more significant. The value obtained for the crossover did not change significantly with the temperature (only for ones higher than 28°C), being around $0.50 \pm 0.02$ V. If in fact the second regime observed at high temperatures is either SCLC or ST and not TFL, then it would explain why the crossover did not change significantly, and more importantly it would mean that for higher temperatures the crossover voltage is not the $V_{TFL}$, but rather the voltage at which the SCLC or the Shallow Trap Regime starts. Although, assuming that the $V_{TFL}$ would be around 0.5 V, $p_{t,0}$ and $n_0$ would take the values $(4.4 \pm 0.2) \times 10^{12}$ cm$^{-3}$ and $(1.5 \pm 0.1) \times 10^9$ cm$^{-3}$, respectively.

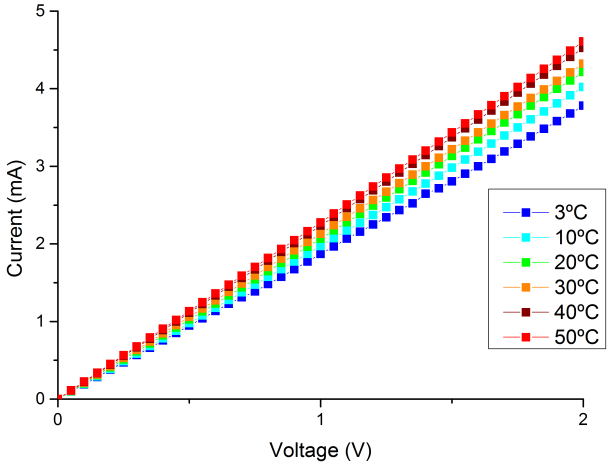


Figure 8: Current-Voltage curves of MEFT4 at various temperatures.

Regarding the thin film, MEFT4, the IV curves obtained are in figure 8, where the sample behaved always as ohmic. The contact distance between these two samples varies by a factor of 30, and so the electric field inside the samples varies by the same amount. Therefore, if the TFL regime in MEFT4 were to happen at the same magnitude of the electric field as in PS3, it means that the range in voltage had to go up to 15 V - 20 V in order to observe

this high-slope regime.

4.5. Transient Photocurrent

The current decays for different temperatures are shown in figure 9 for PS3 and MEFT4. While the photocurrent decay curves for the MEFT4 are quite similar, the curves of PS3 at 10°C and 50°C differ by almost an order of magnitude. The photo response of the nanowires changed significantly with temperature, where at 10°C the sensitivity to light was lower. Note that for every temperature the time of exposure to light was kept the same. A possible reason to explain this is to say that low temperatures favour the adsorption of molecules on the surfaces. Since the high photo response reported on the ZnO nanowires has been attributed to the photodesorption of oxygen molecules $O_2$ [7, 8, 9]. In the dark, oxygen is adsorbed on the ZnO surface defects capturing electrons, which is illustrated in continuous lines in figure 10. As the adsorbed molecules are charged a depletion region is created, bending the conduction and valence band. Once light with energy above the band gap energy is shone on the sample, the photogenerated holes discharge the adsorbed oxygen molecules (dashed line in fig. 10) and hence leading to the desorption of oxygen and the trapping of the hole. As a result, the recombination rate of the photogenerated electrons reduces, their lifetime increases and consequently the current increases as well, owing to the unbalanced concentration of both carriers. However, if the adsorption rate is favoured, in other words if it increases, the lifetime of the photogenerated electrons will be shortened. Therefore this might be the reason for the low photo response observed at 10°C in PS3. This effect, due to the larger surface to volume ratio is more relevant to the nanowires than to the thin film.

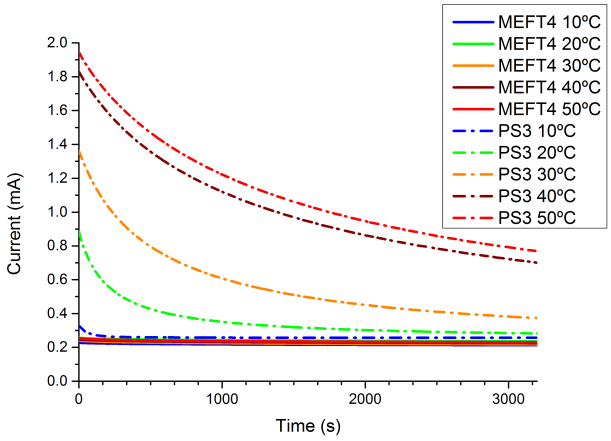


Figure 9: Transient photocurrent of PS3 and MEFT4.

When deconvoluted the transient curve yielded two peaks at 0.85 eV and 0.95 eV, in both samples. To convert lifetime of the observed peaks into energy, the following expression was used $\tau = 10^{13} \exp\left(\frac{E}{kT}\right)$. The second peak was also reported in [7] with ZnO thin film and using the same deconvolution method. Both peaks change in magnitude with temperature for the PS3, whereas for the MEFT4 they did not change significantly. Thus, it is likely that these peaks are associated with surface adsorption, rather than with intrinsic defects, as the thin film is not so sensible to surface effects as the nanowire structure. Each peak might be associated to the adsorption of two different molecules, or with two possible lattice sites where the same molecule can establish a chemical bond. The experiment that we carried out does not allow us to make further conclusions. In order to do so, the surrounding atmosphere has to be controlled.

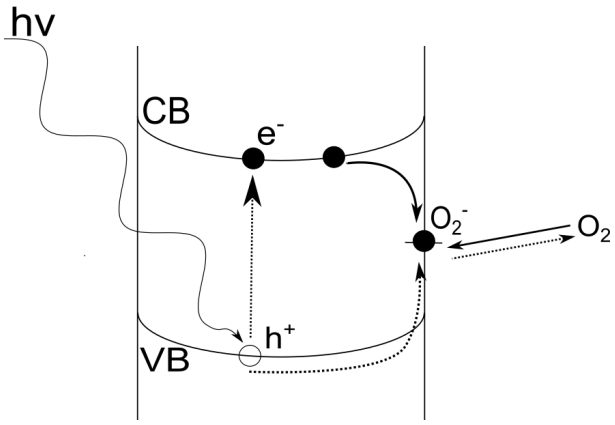


Figure 10: Illustration of the adsorption (continuous line) and desorption (dashed line) of oxygen molecule.

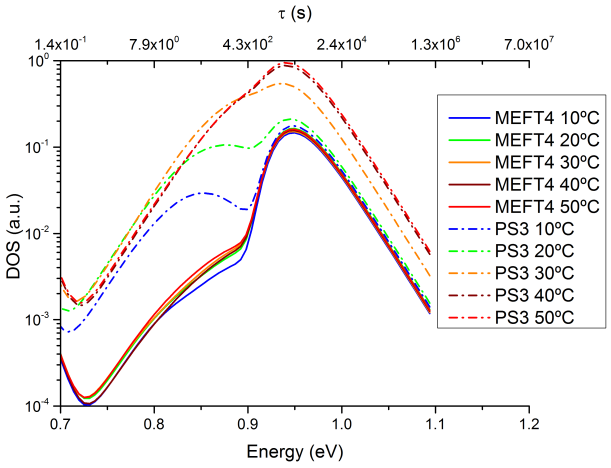


Figure 11: Density of States obtained from Transient Photocurrent of PS3 and MEFT4.

### 4.6. Admittance Spectroscopy

Except for the nanowire sample PS3 at 10°C and 20°C, at lower frequencies the capacitance present a positive slope, which is not expected by the theory. Thus, this might be due to a limitation in the impedance analyser to read low capacitances at lower frequencies, particularly lower than 100 Hz.

In both cases, at atmospheric pressure or in vacuum, both samples have a peak around 300 Hz and 400 Hz, and PS3 has a second peak at 6 kHz while MEFT4 has one at 40 kHz. However, the first one can be an artefact due to the limitation of the analyser at low frequencies, and this "jump" in capacitance might be the point where the device starts reading correctly. At atmospheric pressure and 10°C, instead of a peak near the 350 Hz, PS3 showed a broader peak centred at 200 Hz. Once again except for the sample PS3 at 10°C and 20°C, there are no meaningful changes in the spectrum of both samples between atmospheric pressure and in vacuum. Therefore, the defects detected are likely to be intrinsic ones instead of being due to surface trapping. Further, the peaks at 6 kHz for nanowires and 40 kHz for thin film, may be due to intrinsic defects favoured by the respective growth method used. The nanowires were grown by wet chemical process while the thin film by PLD.

Using the same expression as in TPC that relates the lifetime of a trap with its distance in energy from the nearest band, the energy of these peaks were estimated and then compared with values for intrinsic defects in [10]. The peak observed in PS3 at 6 kHz with 0.48±0.02 eV was associated to singly charged or neutral zinc interstitial ($Zn_i^+$ or $Zn_i$). And the one at 40 kHz or $0.44 \pm 0.02$ eV observed in MEFT4 was associated to neutral zinc interstitial ($Zn_i$).

The figure 16 shows all four trap states identified in this work by transient photocurrent and admittance spectroscopy, in their respective location inside the band gap.

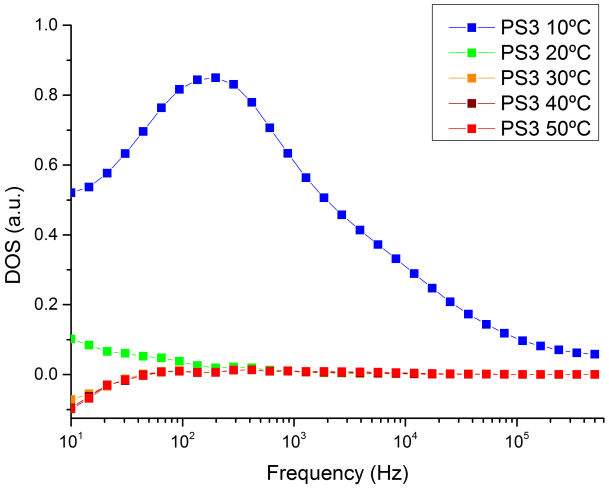


Figure 12: Density of States from Admittance Spectroscopy of PS3 at atmospheric pressure.

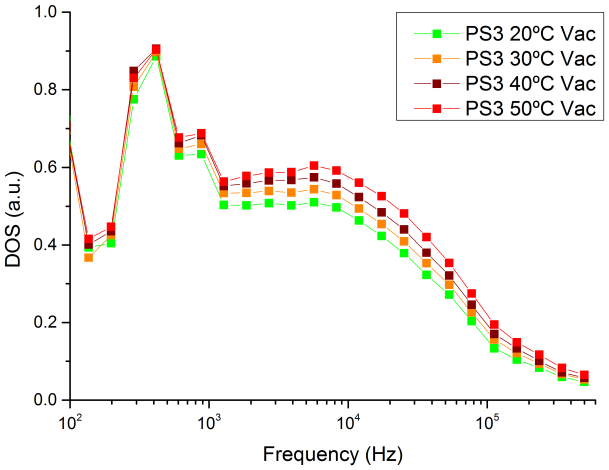


Figure 13: Density of States from Admittance Spectroscopy of PS3 in vacuum.

## 5. Conclusions

Nanowire samples were grown by wet chemical process and their characteristics were compared with a thin film grown by PLD. Morphology of the nanowires was revealed by SEM images, which presented a wide variety of flakes, nanowires, and crystallites. Photocurrent spectroscopy showed that nanowire samples have a band gap of $3.2 \pm 0.3$ eV and a small Urbach tail may indicate a good crystalline structure.

We observed a strong variation of power law exponent as a function of temperature and applied electric field, on the IV curves. It was not possible to estimate the temperature dependence of $V_{TFL}$, due to the limitation of measuring at low temperatures, and this way observe any change in the value of the concentration of unoccupied traps $p_{t,0}$. However, we estimated it to be around $p_{t,0} = (4.4 \pm 0.2) \times 10^{12}$ cm$^{-3}$ and the concentration of carriers to be $n_0 = (1.5 \pm 0.1) \times 10^9$ cm$^{-3}$, assuming $V_{TFL} = 0.5$ V.

Combining transient photocurrent decay and admittance spectroscopy a wide range of time scales of trap lifetimes were probed, from 1 to $3 \times 10^3$ seconds with transient photocurrent and from $10^{-5}$ to $10^{-2}$ seconds with admittance spectroscopy. Two peaks were identified in transient photocurrent and attributed to surface trapping. These peaks were estimated with an energy of 0.85 eV and 0.95 eV, and they might be due to two different molecules adsorption on the surface or to a single molecule species, for instance oxygen, chemically bonding in two different sites in the ZnO lattice. Considering the model proposed to explain the photoconductiv-

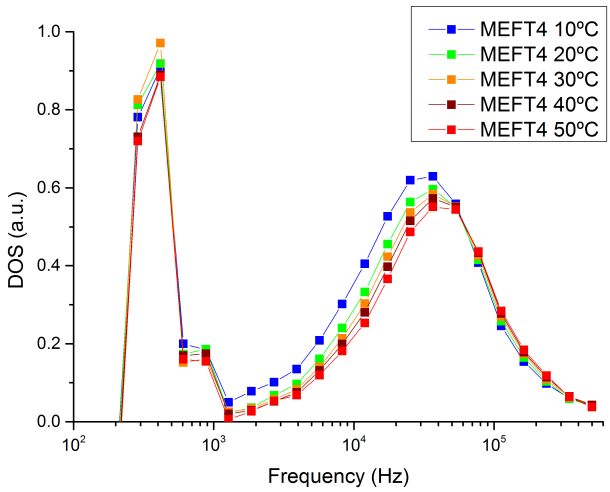


Figure 14: Density of States from Admittance Spectroscopy of MEFT4 at atmospheric pressure.

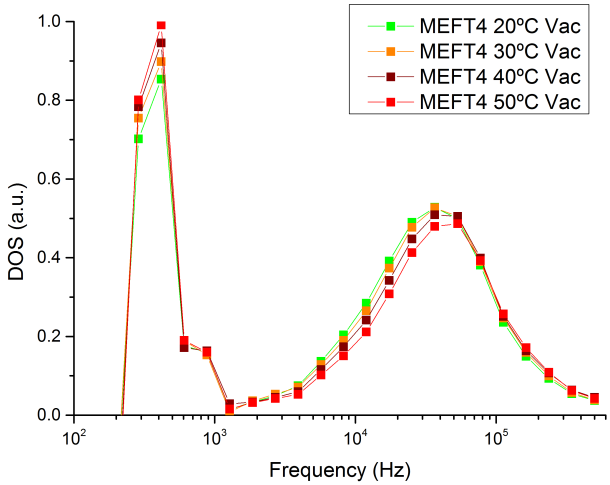


Figure 15: Density of States from Admittance Spectroscopy of MEFT4 in vacuum.

ity of the nanowires, it was concluded that the concentration of unoccupied traps $p_{t,0}$ increases with temperature. That is, these traps may be regarded as the adsorbed oxygen molecules that adsorb to the surface, capturing an electron from the conduction band, and the change in trap concentration may be regarded as how much the adsorption is favoured with temperature.

The admittance spectroscopy of both samples showed a peak at 350 Hz, which might be an artefact. Additionally PS3 had a peak at 6 kHz (0.48±0.02 eV) while MEFT4 at 40 kHz (0.44±0.02 eV), which were associated with intrinsic defects, namely to singly charged or neutral zinc interstitial ($Zn_i^+$ or $Zn_i$) and neutral zinc interstitial ($Zn_i$), respectively.

In the IV curves and in the TPC experiments, PS3 changed its behaviour around 30°C - 40°C

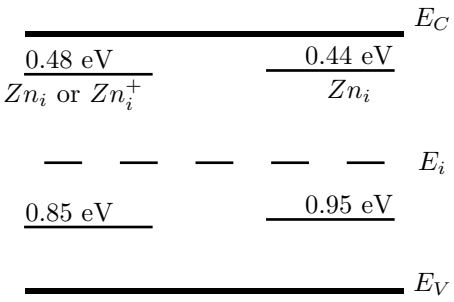


Figure 16: Trap states identified with Transient Photocurrent and Admittace Spectroscopy.

while in the admittance spectroscopy its behaviour changed from 10°C to 20°C. This can be due to fatigue of the sample, as the experiments were carried by the same order as exposed in this work, hence admittance spectroscopy was the last experiment performed. On the other hand, the surrounding atmosphere was not monitored throughout this work. Thus, this shift in temperature at which the sample changes its behaviour, might be owed to the variations of the air composition, such as humidity. Further, the TPC suggested a higher increase in $p_{t,0}$ than it was observed in IV curves, remember that $V_{TFL}$ is proportional to $p_{t,0}$. Consequently, it is suggested as a future work to perform these experiments in a controlled surrounding atmosphere, as well as in vacuum for the case of IV characterization and transient photocurrent. This would allow to answer the question just mentioned, and the one raised the TPC about the origin of the two peaks. A similar approach was used in [8], where the persistent photoconductivity (or PPC effect) of single ZnO nanowire was investigated as a function of the surrounding atmosphere. The experiments were performed in vacuum, and in Argon and Nitrogen atmospheres. This is similar to what was described in this work as TPC. However, in this publication only the decay rates were studied and the density of states related to the decay were not.

Concerning the capability of these samples as energy harvesters, we presented a model and simulation results of the voltage yielded by a single nanowire, when it is compressed or bent. Using the developed model the compression configuration was shown to be the most efficient. Experiments, however, will have to be done in a later stage

**Acknowledgements**
I would like to acknowledge my supervisor, Prof. Reinhard Schwarz, and co-supervisor, Prof. Rachid Ayouchi for accepting me as their student and for their invaluable support, guidance and ideas throughout all this work.

Besides my supervisors, I would like to express my gratitude to Dr. Tânia Braz for all the discussions we had and who was always willing to help. Also a worthy mention is Prof. Umesh Mardolcar for his help and contribution, throughout my entire dissertation work, for the admittance spectroscopy measurements and for the assembly of the vacuum system.

My sincere thanks also goes to Prof. Pedro Sanguino and Prof. Ricardo Franco for preparing the nanowire samples.

Finally, I would like to thank my family and friends, who were always supporting me and encouraging me with theirs best wishes.

**References**

[1] Z. Fan and J. G. Lu. Zinc oxide nanostructures: synthesis and properties. *Journal of nanoscience and nanotechnology*, 5(10):1561–73, oct 2005.

[2] C. Klingshirn. ZnO: material, physics and applications. *Chemphyschem : a European journal of chemical physics and physical chemistry*, 8(6):782–803, apr 2007.

[3] Z. L. Wang and J. Song. Piezoelectric nanogenerators based on zinc oxide nanowire arrays. *Science (New York, N.Y.)*, 312(5771):242–6, apr 2006.

[4] S. Xu and Z. L. Wang. Oxide nanowire arrays for light-emitting diodes and piezoelectric energy harvesters. *Pure and Applied Chemistry*, 83(12):2171–2198, jan 2011.

[5] M. Lampert and P. Mark. *Current injection in solids*, volume 170. Academic Press, 1970.

[6] R. L. Johnson. *Characterization of piezoelectric ZnO thin lms and the fabrication of piezoelectric micro-cantilevers*. PhD thesis, 2005.

[7] S. a. Studenikin, N. Golego, and M. Cocivera. Improved Laplace transform method to determine trap densities from transients: application to ZnO and films. *Semiconductor Science and Technology*, 13(12):1383–1391, 1999.

[8] D. Cammi and C. Ronning. Persistent Photoconductivity in ZnO Nanowires in Different Atmospheres. *Advances in Condensed Matter Physics*, 2014:2–7, 2014.

[9] C. Soci, a. Zhang, B. Xiang, S. a. Dayeh, D. P. R. Aplin, J. Park, X. Y. Bao, Y. H. Lo, and D. Wang. ZnO nanowire UV photodetectors with high internal gain. *Nano letters*, 7(4):1003–9, apr 2007.

[10] M. Willander, O. Nur, J. R. Sadaf, M. I. Qadir, S. Zaman, A. Zainelabdin, N. Bano, and I. Hussain. Luminescence from zinc oxide nanostructures and polymers and their hybrid devices. *Materials*, 3(4):2643–2667, 2010.